THE JOURNAL OF PHYSICAL CHEMISTRY C

Article

Cite This: J. Phys. Chem. C 2018, 122, 18070−18076

pubs.acs.org/JPCC

Stability and Electronic Properties of PtPd Nanoparticles via MD and DFT Calculations

I. V. Chepkasov,*[,†] M. A. Visotin,[‡] E. A. Kovaleva,[§] A. M. Manakhov,[∥] V. S. Baidyshev,[†] and Z. I. Popov[∥]

[†]Katanov Khakas State University, 90 Lenin pr., 655017 Abakan, Russia

[‡]Kirensky Institute of Physics, 50/38 Akademgorodok, 660036 Krasnoyarsk, Russia

[§]Siberian Federal University, 79 Svobodny pr., 660041 Krasnoyarsk, Russia

[∥]National University of Science and Technology MISiS, 4 Leninskiy pr., 119049 Moscow, Russia

Supporting Information

ABSTRACT: The structural as well as electronic properties of PtPd nanoparticles (NPs) were investigated by using molecular dynamics simulations and density functional theory calculations. A wide range of NPs of different sizes (from 1.5 to 4 nm), structures (core−shell, alloy, Janus), and compositions were taken into consideration. It was shown that PtPd NPs of less than ∼2.0 nm are prone to structural transformations to icosahedral (Ih) shape, regardless of their initial structure and composition. On the other hand, for NPs of size ∼2.5 nm, the increase of temperature up to 700−900 K leads to structural changes only for compositions close to 40% Pt, which corresponds to energetic minimum for Pt@Pd NPs. The Ih form of Pd@Pt NPs with monolayer thickness of Pt on the surface appears to have the most negatively charged surface which makes this kind of NPs the best candidate for catalysis application.

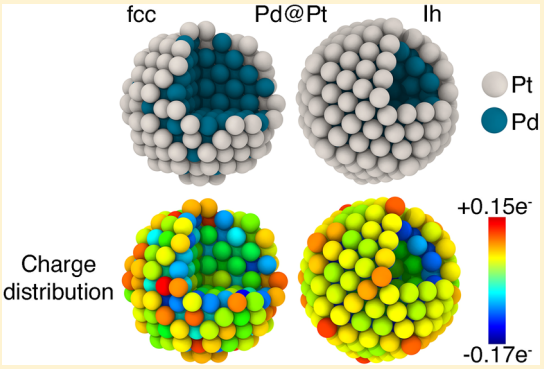

1. INTRODUCTION

The discovery of gold nanoparticles (NPs) catalytic properties has attracted much research attention to the study of NP-based catalysts.[1] Although the main attention was paid to the search for correlation between the catalytic activity and particle size for a long time, the atomic and electronic structure of NPs plays a significant role in determining their catalytic activity.[2] Tuning of NP parameters like faceting, size, composition, and phase can improve their catalytic properties.[3]

Platinum is known to be the most commonly used material for catalytic application for the hydrogen oxidation reaction and oxygen reduction reaction (ORR).[4,5] However, vast research activity is devoted to the search for a cheaper but still effective alternative for this expensive material. As a solution, platinum-based multicomponent NPs have been also proposed. Bimetallic NPs like PtAu, PtCu, PtCo, and PtRh demonstrate higher electrocatalytic activity and longer lifetime in CO oxidation reaction and ORR than monometallic Pt NPs do.[6−10] Mass-specific activity of PtAu/C was reported to be 3.1−4.9 times larger than that of commercial Pt/C.[11] Among the number of platinum-based nanocatalysts, PtPd nanoalloys exhibit outstanding performance in both high catalytic activity and selectivity and cost reduction. Besides that, they are perspective to improve the oxidation reactions and can be used in low-temperature fuel cells (proton exchange membrane fuel cells and direct methanol fuel cells).[12]

There are four possible structures bimetallic platinum−palladium NPs can form: core−shell Pt@Pd and Pd@Pt (Figure 1a,b), Janus Pt|Pd (Figure 1c), and homogeneous bimetallic alloy Pt−Pd (Figure 1d) NPs. Up to date, only core−shell (Pt@Pd and Pd@Pt) and bimetallic alloy Pt−Pd NPs have been synthesized experimentally.[13−17] The evidence of Janus-type Pt|Pd NPs has not been reported yet.

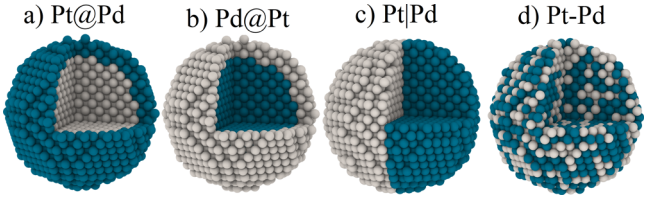

Figure 1. Possible structures of bimetallic NPs: (a) Pd core/Pt shell (Pd@Pt), (b) Pt core/Pd shell (Pt@Pd), (c) Janus (Pt|Pd), and (d) bimetallic alloy (Pt−Pd).

The catalytic activity of PtPd NPs is affected not only by their size but also their Pt/Pd ratio, structure, and shape. In particular, Wu et al.[18] described the nonmonotonic nature of

Received: May 2, 2018
Revised: July 13, 2018
Published: July 13, 2018

DOI: 10.1021/acs.jpcc.8b04177
J. Phys. Chem. C 2018, 122, 18070−18076

PtPd alloy NPs catalytic activity in ORR dependence on atomic composition. While Pt atoms are the active sites for the oxygen adsorption, density functional theory (DFT) calculations, and X-ray photoelectron spectroscopy measurements exhibited that the Pt-poor nanoclusters showed better activity because of the electron transfer from Pd to Pt atoms, whereas the Pt-rich NPs have inferior performance because of the opposite electron transfer. The role of the structure of bimetallic NPs is indicated by enhanced performance of core−shell NPs and even higher boost of catalytic activity in crown-jewel structured nanocrystals compared with disordered alloy NPs.[19,20] The introduction of palladium affects not only the charge on Pt but also the ability of Pt atoms to displace to accommodate O adsorption, which is important for ORR catalysis.[21,22] Besides this, the shape of the NPs also affects their properties with icosahedral (Ih) and decahedral (Dh) shape showing greater catalytic potential than cubic-symmetry forms for both pure Pt,[23,24] Pd@Pt,[25,26] and crown-jewel NPs.[27]

Thus, all structural features like the diameter of particles, size of the core, and shell, Pt/Pd ratio, and surface atom distribution should be taken into account when synthesizing highly active nanocatalysts. Another critical issue is the thermal stability of NPs because most catalysts are usually exposed to high temperatures.[28] Previously, Huang et al.[29,30] investigated the thermal stability of large (6.2 nm) PtPd NPs consisting of 8247 atoms with different structures (core−shell, alloy). It was determined that melting processes in NPs proceed in two stages and depend on the ratio of core and shell sizes. However, it was shown that small NPs (<2−3 nm) can undergo structural changes at much lower temperatures because of the surface effects.[31,32] For example, bimetallic Pd_{147}@Pt_{162} NPs of about 2 nm were synthesized by a homogeneous route.[32] The detailed characterization by in situ extended X-ray absorption fine structure spectroscopy showed that the real composition is in fact inverted with respect to the originally proposed: Pt atoms concentrated in the core, and Pd formed the shell resulting in Pt_{147}@$Pd_{147}Pt_{15}$ particles. This transformation was explained in terms of size effects, in particular, a large number of edge and corner sites. The effect of the size and shape on the stability and activity of Pd@Pt NPs on the ORR was studied by An et al.[33] It was found that with an increase of the size from 1 to 3 nm, the catalytic activity in ORR varies in different ways for NPs of various shape—increase for sphere-like truncated octahedron and decreases for tetrahedron type.[33]

In this work, molecular dynamics (MD) simulations were used to explore the temperature impact on various PtPd NPs with different sizes (D = 1.5; 2; 2.5; 3; 4 nm) and structures (Pt@Pd, Pd@Pt, Pt|Pd, and Pt−Pd alloy). At the same time, DFT was applied for investigations of their electronic properties and charge redistribution, which is crucial for the catalytic activity.

2. SIMULATION METHODOLOGY

Simulation of PtPd NPs annealing was performed by MD modeling using a large-scale atomic/molecular massively parallel simulator (LAMMPS).[34] The MD method is widely used for investigation of structural phase transitions in metals and alloys because it allows computing dynamical characteristics of the simulated system.[35−37] According to the literature, thermodynamic properties and interaction between atoms in metallic NPs can be successfully described by various many-body potentials, namely, Sutton−Chen, Cleri−Rosato, and embedded atom method (EAM) model.[38−40] EAM potential proposed by Zhou et al.[41] was chosen to determine the interaction energy of platinum and palladium atoms, as it proved its ability to describe Pt−Pd NPs.[42,43]

A Nosé−Hoover thermostat was employed to simulate PtPd NPs heating. The velocity Verlet scheme was used for solving the equations of motion with the constant time step h of 1 fs.[44−46] The PtPd NPs structures, created by cutting from face-centered cubic (fcc) lattices, were first optimized and then heated in four steps up to T = 300 K, T = 500 K, T = 700 K, and T = 900 K to test their stability. The lattice parameters for Pt and Pd were 3.92 and 3.89 Å, respectively.[41] For each temperature, simulation time t was set to 5 ns, and heating from one temperature to another took t = 1 ns. Core−shell Pt@Pd particles contained from 10 to 70% Pt atoms, and Pd@Pt particles contained from 30 to 90% platinum atoms. The platinum content in Janus and bimetallic alloy NPs was in the range of 10−90%. In total, for each size, 32 different NPs were considered.

To determine the structural stability of NPs, the energy gain of NPs formation was calculated as the difference between binding energy of NPs and the bulk counterparts.

$$\Delta E = (E_{\mathrm{NPs}} - E_{\mathrm{Pt}}N_{\mathrm{Pt}} - E_{\mathrm{Pd}}N_{\mathrm{Pd}})/(N_{\mathrm{Pt}} + N_{\mathrm{Pd}}) \quad (1)$$

E_{NPs} is the potential energy of the particle, N_{Pt} and N_{Pd} correspond to the number of Pt and Pd atoms, and E_{Pt} and E_{Pd} stand for the potential binding energy for the bulk platinum and palladium, respectively. Potential binding energy for bulk materials was calculated for different temperatures within the NPT ensemble using the same embedded atom potential (see the Supporting Information, Table S1).

The contribution of configurational entropy to the free energy for the Pt−Pd alloy NPs was also considered. The maximum possible entropic contribution per atom was calculated under the assumption that all configurations have the same statistical weight using the following expression[47]

$$T\,\mathrm{d}S = -k_{\mathrm{B}}T[N_{\mathrm{Pt}}\ln\ N_{\mathrm{Pt}} + N_{\mathrm{Pd}}\ln N_{\mathrm{Pd}}] \quad (2)$$

where k_{B} is Boltzmann's constant. However, different atomic configurations have different potential energy values, especially if differences concern the surface of the NP. Therefore, the configurations have different statistical weights, and as a consequence, the actual value of entropic contribution is lower than the calculated dS.[48]

To study the electronic properties of the investigated Pt−Pd NPs, the structures were optimized and charge redistribution was calculated within the framework of DFT using OpenMX software.[49] The core Coulomb potential in OpenMX is replaced by a tractable norm-conserving pseudopotential proposed by Morrison, Bylander, and Kleinman,[50] which is a norm-conserving version of the ultrasoft pseudopotential by Vanderbilt.[51] Small PtPd NPs (321 atoms, D = 2 nm) with different structures (core−shell, alloy, Janus) and compositions were chosen for electronic properties analysis. We used the Bader[52] approach to calculate atomic charge based on the OpenMX results. Energy cutoff for the numerical integration grid was 180 Ry. The results of calculations were postprocessed and visualized using the Open Visualization Tool (OVITO)[53] and VESTA[54].

DOI: 10.1021/acs.jpcc.8b04177
J. Phys. Chem. C 2018, 122, 18070−18076

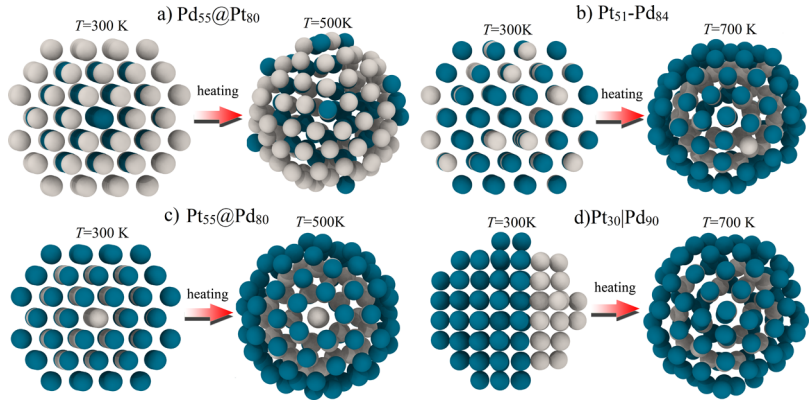

Figure 2. Thermoactivated fcc → Ih structural transition in Pt−Pd NPs, D = 1.5 nm. (a) Pd core/Pt shell, (b) alloy Pt−Pd, (c) Pt core/Pd shell, (d) Janus Pt−Pd. The Pt and Pd atoms are shown by light and dark gray balls, respectively.

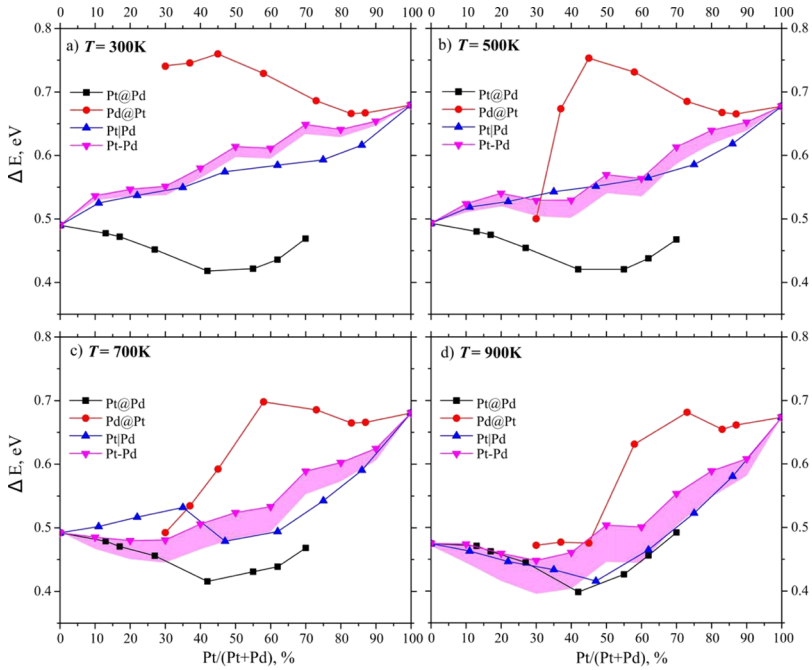

Figure 3. Difference between binding energies in NPs and in the bulk (ΔE, eV) versus platinum percentage in core−shell (Pd@Pt and Pt@Pd), Janus-type (Pt|Pd) and alloy (Pt−Pd) NPs with D = 2 nm at (a) T = 300 K, (b) T = 500 K, (c) T = 700 K, and (d) T = 900 K. Possible contribution of configurational entropy for Pt−Pd alloy NPs is shown as a shaded area under the magenta line.

3. RESULTS AND DISCUSSION

Because heating can cause significant structural changes in small size NPs,[55] the question of thermal stability is very important for the nanocatalyst design. The difference between binding energy of NPs and the bulk was calculated to study the thermodynamical stability of NPs as a function of temperature. For all NPs of the same composition, according to this eq 1, lower total energy inevitably leads to lower ΔE and thus determines better structural stability. According to the results of various Pt−Pd NPs thermal stability estimations, the ones with D = 1.5 nm are the most structurally unstable amongst all considered. All four possible structures undergo structural transition to the Ih phase (see Figure 2) even at 500−700 K. This can be explained in terms of pentagonal symmetry as the most stable for small Pt−Pd clusters according to the first-principle calculations.[56,57] Only 4 of 32 particles with D = 2 nm NPs transformed from fcc to Ih and Dh phase. Pd@Pt NPs with a Pt content less than 50% changed their structure. According to our calculations this structure of a particle (Pd core, Pt shell) is more energetically unstable. Figure 3 shows the dependences of ΔE for D = 2 nm NPs on Pt percentage at different temperatures (see the Supporting Information for D = 1.5, 2.5, 3, 4 nm). Possible contribution of configurational entropy for Pt−Pd alloy NPs is also shown as a shaded area under the corresponding graph (because the T dS value from 2 is a maximum estimate, the actual free energy lies inside the shaded region). As can be clearly seen, Pt@Pd is the most stable at room temperature, in agreement with previously reported MD[30] and DFT[58] results. Increase of the temperature from 300 to 500 K leads to the structural changes in less energetically favorable Pd@Pt particles in the first place. Pd_{225}@Pt_{96} undergoes fcc → Dh transition at T = 500 K (Figure 3b, Pd@Pt, Pt—30%) which leads to significant decrease of ΔE. Thermally activated structural transition to icosahedra is observed at 700 and 900 K for Pt@Pd NPs with 40% platinum content (Figure 3c,d), and the resulting structure corresponds to the lowest ΔE. This agrees well

DOI: 10.1021/acs.jpcc.8b04177
J. Phys. Chem. C 2018, 122, 18070−18076

with previous Pt−Pd NPs calculations performed by Paz-Borbon et al.,[56] where the energy minimum was shown to correspond to the Pt content of 43% in Ih clusters with Pd atoms on surface. In general, Pt@Pd core−shell particles appear to be the most stable ones. Despite that at higher temperatures, alloy NPs with a low Pt content seem to be more favorable in terms of free energy, there was no transformations from Pt@Pd to disordered alloy Pt−Pd or dissolution of Pt core in surrounding palladium shell. No isomorph transitions were observed for $D > 2.5$ nm, regardless the structure and Pt/Pd ratio.

Detailed investigation of structural changes in PtPd NPs showed that core−shell Pd@Pt and Janus Pt|Pd particles are significantly rearranged at temperatures more than 700 K. Platinum is then concentrated in the center of the particle, whereas palladium atoms are predominantly localized on the surface, as can be clearly seen in Figure 4 at $T = 700$ K and $T = 900$ K. The tendency of Pd atoms diffusion from the bulk to the surface can be explained in terms of the difference in surface energies for platinum and palladium which was experimentally observed by Bernardi et al.[59] for PtPd NPs with D from 3.8 to 4.8 nm at different temperatures. Average surface energy values (2.49 J/m^2 for Pt and 2.00 J/m^2 for Pd)[60] show that Pd coverage of NPs surface is more thermodynamically favorable than Pt. This corresponds well to the ΔE values of bare platinum and palladium NPs ($\Delta E = 0.679$ eV for Pt, $\Delta E = 0.489$ eV for Pd).

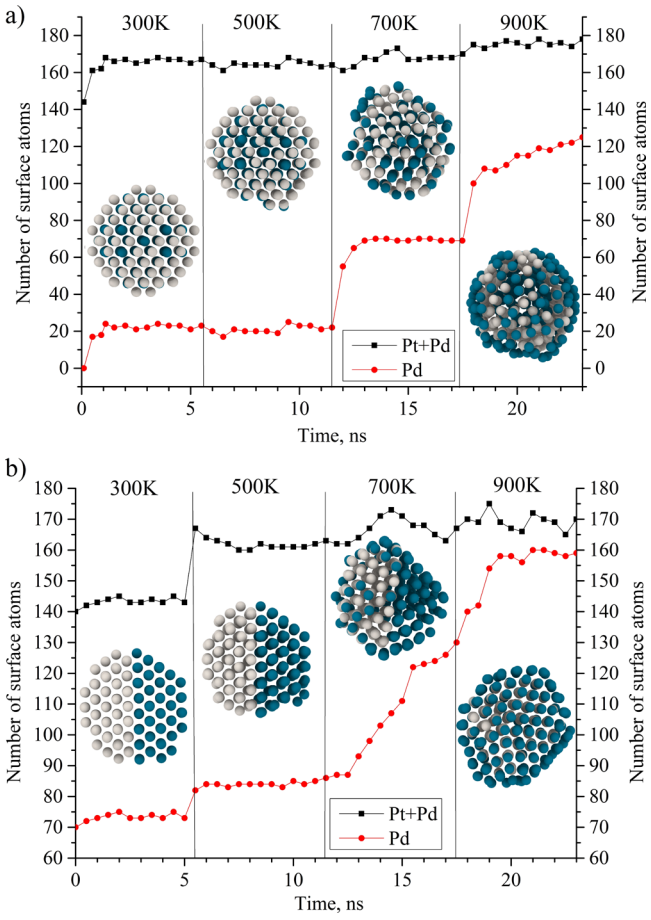

Figure 4. Temperature dependence of the number of surface atoms in 2 nm Pt−Pd NPs: (a) Core−shell $Pd_{177}@Pt_{144}$ and (b) Janus $Pt_{156}|Pd_{165}$. The Pt and Pd atoms are shown by light and dark gray balls, respectively.

Different scenarios were determined for Pt and Pd atoms redistribution in NPs with different structure. For instance, bimetallic alloy (Pt−Pd) and Pd@Pt NPs are changed because of Pd atoms diffusion from the bulk to the surface and Pt diffusion from the surface to the bulk (see Figure 4a). In contrast, Pd atoms migrate along the whole surface of Janus particles gradually moving to the platinum hemisphere and forming a palladium shell (see Figure 4b). Janus NPs with $D > 2.5$ nm transform to the nonsymmetric Pt@Pd NPs with the core center being displaced from the shell center. Similar effects of Pd atoms diffusion into the shell were experimentally observed in the Pd@Pt NPs. Paes et al.[61] synthesized Pd@Pt NPs with sizes from 4 to 5 nm and all of the synthesized core@shell NPs were proven to have the structure of Pd@PtPd.

Pt@Pd NPs with $D > 2.5$ nm do not undergo any significant structural changes at four temperatures studied (300, 500, 700, and 900 K). To investigate higher temperatures close to the melting point, the particles were gradually heated from $T = 100$ K to $T = 2000$ K for $t = 20$ ns. Pt@Pd structures are the most interesting to describe. The diffusive rearrangement of atoms and facets formation at the surface of $Pt_{249}@Pd_{306}$ particles at $T = 1090$ K was observed. The particle shape changes at $T = 1150$ K becoming polyhedral and decreasing the potential energy because of the decrease of its surface contribution. Polyhedral core−shell NPs were also observed experimentally.[62,63] Pd@Pt and bimetallic alloy Pt−Pd are different from the previous ones when heated. In $Pd_{55}@Pt_{500}$ and $Pt_{733}Pd_{226}$ NPs similar to $Pt_{249}@Pd_{306}$ cluster, potential energy and heat capacity fluctuations were observed at ∼850 K because of the internal rearrangements in NPs. However, it did not lead to the change of the structure and shape of the particles below the melting temperature. Nevertheless, Pd atoms diffuse actively to the surface after the melting and decrease the potential energy. The process of PtPd NPs melting was described in detail in our recent work.[64]

To investigate the influence of the NP structure on its electron density distribution, a series of DFT calculations were performed using OpenMX software followed by the Bader charge analysis.[52] Figure 5 shows the dependences of average surface charge on the Pt percentage for three different NPs

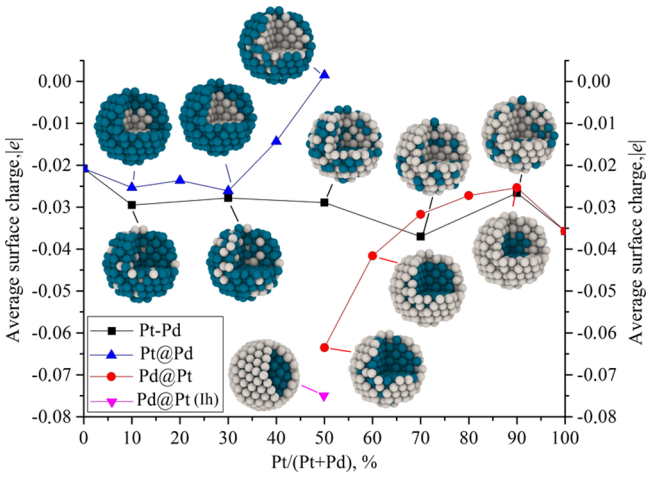

Figure 5. Average surface charge of the Pt−Pd NPs vs Pt content. The Pt and Pd atoms are shown by light and dark gray balls, respectively (white and cyan balls in color version).

DOI: 10.1021/acs.jpcc.8b04177
J. Phys. Chem. C 2018, 122, 18070−18076

structures. Because the DFT calculations are computationally demanding, small PtPd NPs (321 atoms, D = 2 nm) with different structures were chosen for electronic properties analysis. Several Pt core/Pd shell clusters were studied (from 10 to 50% Pt). NPs with higher Pt percentage of 60 and 70% were excluded because palladium atoms do not cover the whole NPs in those cases. Similarly, the Pt content varied from 90 to 50% for the Pd core/Pt shell structure. Five different bimetallic alloy Pt−Pd NPs with random atom distribution were considered (from 90 to 10% Pt).

The difference between surface charge of pure Pt and Pd NPs which is equal to 0.015e is shown in Figure 5. This value agrees well with the work function difference of these types of atoms.[65] In all considered cases, negative charge is localized on the surface of NPs, except for the cubic structured Pt@Pd particles with small positive surface charge of +0.0015e (see Figure 5). Pt@Pd and Pd@Pt NPs demonstrate the opposite trend because of the moving of Pt−Pd (Pd−Pt) boundary from the center to the particle surface. Indeed, the decrease of Pt layers covering Pd core leads to the increase of the number of electrons on the surface for Pd@Pt and vice versa. From our results, it can be concluded that covering of Pd NPs with monoatomic layer of Pt atoms can increase the surface charge by a factor of two with respect to the pure Pt particle or it is three times higher than pure Pd NPs surface. These results correspond well with previous finding of charge transfer in core−shell Pd@Pt NPs is directed from Pd to Pt.[18,58] While the explanation of enhanced catalytic activity of the Pt atoms in NPs, for example, in oxygen adsorption reaction is related to the ability of Pt to donate electrons to oxygen,[16] the localization of excess electronic density on the surface of NPs can lead to enhancement of its catalytic activity.[66,67] The opposite situation is observed when Pt NPs are coated with a monoatomic layer of Pd. Considering that Pd tends to occupy a position predominantly on the surface of the NPs under heating, one must carefully select the application areas of such NPs because palladium in this case acts as a shield leading to a decrease surface charge in the NPs.

The investigation of electronic properties of Ih PtPd NPs showed an increase of the average surface charge compared with fcc PtPd NPs. According to our calculations, the increase of the average surface charge for Ih monodisperse NPs of Pt and Pd in comparison with the fcc structure is 27% (from −0.0357e for Pt_{fcc} to −0.0454e for Pt_{Ih}) and 39% (from −0.0208e for Pd_{fcc} to −0.0289e for Pd_{Ih}), respectively. Among all of the investigated NPs, the largest electronic density excess on the surface was observed in the Ih particle where the core of Pd was covered by a monolayer of Pt, the average surface charge increased by 18% (from −0.0635e for $Pd@Pt_{fcc}$ to −0.0749e for $Pd@Pt_{Ih}$) (see Figure 5). For the Ih particles with Pt core covered by the Pd monolayer, the charge changes from +0.0015e for $Pt@Pd_{fcc}$ to −0.0001e for $Pt@Pd_{Ih}$ (Figure 6).

4. CONCLUSION

The MD simulations and DFT calculations were used to investigate the equilibrium structures, thermal stability, and electronic properties of Pt−Pd NPs. Small Pt−Pd clusters less than ∼2.0 nm in diameter tend to form Ih structures, regardless their initial structure and composition. This may increase the catalytic efficiency of NPs, as we show that Ih Pt-based NPs are known to be more catalytically active in comparison with fcc structures. The number of structural transitions to the Ih form decreases significantly with the increase of the NP size and vanishes as it reaches 2.5 nm. However, another kind of structural changes, namely, the redistribution of Pd atoms from the bulk to the surface, was observed at the temperatures higher than 700 K. This effect may be explained in terms of the surface formation energy difference for platinum and palladium. Core−shell Pd@Pt and Janus Pt|Pd NPs were found to be the least stable amongst all, even for the temperatures much lower than their melting temperature. Janus Pt|Pd NPs transform to Pt@Pd ones with the temperature increase through Pd atoms diffusion along the surface of the particles. Investigation of the electronic properties of PtPd NPs with various structures showed that the highest electron density on the surface is formed in an Ih particle where Pd core coated with a monolayer of Pt. Fixed notion about direct relation between catalytic activity and surface charge lead us to claim that $Pd@Pt_{Ih}$ NPs will be the most promising candidate for catalytic applications from the whole range of considered NPs.

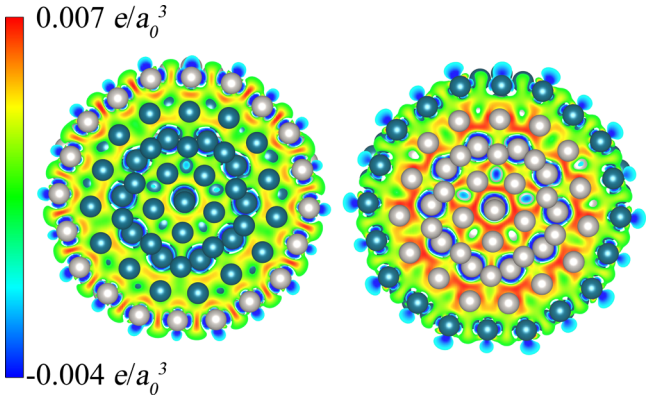

Figure 6. Difference electron density for Ih structure of Pd@Pt(left) and Pt@Pd (right) taken from superposition of atomic densities of constituent atoms. The Pt and Pd atoms are shown by light and dark gray balls, respectively. a_0 equals to Bohr radius.

■ ASSOCIATED CONTENT

Supporting Information

The Supporting Information is available free of charge on the ACS Publications website at DOI: 10.1021/acs.jpcc.8b04177.

Difference between binding energies in NPs and in the bulk (ΔE, eV) versus platinum percentage in Pt−Pd NPs with different structures and diameters (1.5, 2.5, 3, and 4 nm) and at different temperatures (300, 500, 700, and 900 K) (PDF)

■ AUTHOR INFORMATION

Corresponding Author

*E-mail: ilyachepkasov@gmail.com.

ORCID

I. V. Chepkasov: 0000-0001-8376-2999
M. A. Visotin: 0000-0003-2265-9394
A. M. Manakhov: 0000-0003-4517-1682

Notes

The authors declare no competing financial interest.

DOI: 10.1021/acs.jpcc.8b04177
J. Phys. Chem. C 2018, 122, 18070−18076

■ ACKNOWLEDGMENTS

The authors are grateful to Vladislav A. Kalyuzhny for the assistance with the computational resources. The research is carried out using the equipment of the shared research facilities of HPC computing resources at Lomonosov Moscow State University and resources of the Center for the Information and Computing of Novosibirsk State University. The work was supported by the Russian Foundation for Basic Research (RFBR no. 17-42-190308-r) and Foundation for Assistance to Small Innovative Enterprises (FASIE) (Project no. 0033625). E.A.K. would also like to thank the Ministry of Education and Science of the Russian Federation (the government contract to Siberian Federal University, grant no. 16.1455.2017/PCh) and the Foundation for Assistance to Small Innovative Enterprises (FASIE) (Project no. 0033639).

■ REFERENCES

(1) Haruta, M.; Yamada, N.; Kobayashi, T.; Iijima, S. Gold Catalysts Prepared by Coprecipitation for Low-Temperature Oxidation of Hydrogen and of Carbon Monoxide. *J. Catal.* **1989**, *115*, 301−309.
(2) Zhang, C.; Shen, X.; Pan, Y.; Peng, Z. A Review of Pt-Based Electrocatalysts for Oxygen Reduction Reaction. *Front. Energy* **2017**, *11*, 268−285.
(3) Cao, S.; Tao, F. F.; Tang, Y.; Li, Y.; Yu, J. Size- and shape-dependent catalytic performances of oxidation and reduction reactions on nanocatalysts. *Chem. Soc. Rev.* **2016**, *45*, 4747−4765.
(4) Lu, S.; Zhuang, Z. Investigating the Influences of the Adsorbed Species on Catalytic Activity for Hydrogen Oxidation Reaction in Alkaline Electrolyte. *J. Am. Chem. Soc.* **2017**, *139*, 5156−5163.
(5) Nie, Y.; Li, L.; Wei, Z. Recent Advancements in Pt and Pt-Free Catalysts for Oxygen Reduction Reaction. *Chem. Soc. Rev.* **2015**, *44*, 2168−2201.
(6) Luo, L.; Duan, Z.; Li, H.; Kim, J.; Henkelman, G.; Crooks, R. M. Tunability of the Adsorbate Binding on Bimetallic Alloy Nanoparticles for the Optimization of Catalytic Hydrogenation. *J. Am. Chem. Soc.* **2017**, *139*, 5538−5546.
(7) Barım, Ş. B.; Bozbağ, S. E.; Yu, H.; Kızılel, R.; Aindow, M.; Erkey, C. Mesoporous Carbon Aerogel Supported PtCu Bimetallic Nanoparticles via Supercritical Deposition and Their Dealloying and Electrocatalytic Behaviour. *Catal. Today* **2017**, *310*, 166−175.
(8) Zhang, M.; Shi, J.; Ning, W.; Hou, Z. Reduced Graphene Oxide Decorated with PtCo Bimetallic Nanoparticles: Facile Fabrication and Application for Base-Free Oxidation of Glycerol. *Catal. Today* **2017**, *298*, 234−240.
(9) Hersbach, T. J. P.; Kortlever, R.; Lehtimäki, M.; Krtil, P.; Koper, M. T. M. Local Structure and Composition of PtRh Nanoparticles Produced Through Cathodic Corrosion. *Phys. Chem. Chem. Phys.* **2017**, *19*, 10301−10308.
(10) Beermann, V.; Gocyla, M.; Willinger, E.; Rudi, S.; Heggen, M.; Dunin-Borkowski, R. E.; Willinger, M.-G.; Strasser, P. Rh-Doped Pt-Ni Octahedral Nanoparticles: Understanding the Correlation between Elemental Distribution, Oxygen Reduction Reaction, and Shape Stability. *Nano Lett.* **2016**, *16*, 1719−1725.
(11) Ma, Y.; Zhang, H.; Zhong, H.; Xu, T.; Jin, H.; Geng, X. High active PtAu/C catalyst with core-shell structure for oxygen reduction reaction. *Catal. Commun.* **2010**, *11*, 434−437.
(12) Long, N. V.; Thi, C. M.; Yong, Y.; Nogami, M.; Ohtaki, M. Platinum and Palladium Nano-Structured Catalysts for Polymer Electrolyte Fuel Cells and Direct Methanol Fuel Cells. *J. Nanosci. Nanotechnol.* **2013**, *13*, 4799−4824.
(13) Peng, L.; van Duyne, R. P.; Marks, L. D. Compositional Inhomogeneity and Corner Enrichment of Pt in Pt/Pd Bimetallic Nanoparticles. *J. Phys. Chem. C* **2016**, *120*, 21069−21075.
(14) Yin, A.-X.; Min, X.-Q.; Zhu, W.; Wu, H.-S.; Zhang, Y.-W.; Yan, C.-H. Multiply twinned Pt-Pd nanoicosahedrons as highly active electrocatalysts for methanol oxidation. *Chem. Commun.* **2012**, *48*, 543−545.
(15) Khanal, S.; Casillas, G.; Velazquez-Salazar, J. J.; Ponce, A.; Jose-Yacaman, M. Atomic Resolution Imaging of Polyhedral PtPd Core-Shell Nanoparticles by Cs-Corrected STEM. *J. Phys. Chem. C* **2012**, *116*, 23596−23602.
(16) Liang, Y.; Ou, C.; Zhang, H.; Ding, X.; Zhao, M.; Wang, J.; Chen, Y. Advanced Insight into the Size Effect of PtPd Nanoparticles on NO Oxidation by in Situ FTIR Spectra. *Ind. Eng. Chem. Res.* **2018**, *57*, 3887−3897.
(17) Tao, F.; Grass, M. E.; Zhang, Y.; Butcher, D. R.; Renzas, J. R.; Liu, Z.; Chung, J. Y.; Mun, B. S.; Salmeron, M.; Somorjai, G. A. Reaction-Driven Restructuring of Rh-Pd and Pt-Pd Core-Shell Nanoparticles. *Science* **2008**, *322*, 932−934.
(18) Wu, J.; Shan, S.; Cronk, H.; Chang, F.; Kareem, H.; Zhao, Y.; Luo, J.; Petkov, V.; Zhong, C.-J. Understanding Composition-Dependent Synergy of PtPd Alloy Nanoparticles in Electrocatalytic Oxygen Reduction Reaction. *J. Phys. Chem. C* **2017**, *121*, 14128−14136.
(19) Zhang, H.; Watanabe, T.; Okumura, M.; Haruta, M.; Toshima, N. Crown Jewel Catalyst: How Neighboring Atoms Affect the Catalytic Activity of Top Au Atoms? *J. Catal.* **2013**, *305*, 7−18.
(20) Zhang, H.; Toshima, N. Crown Jewel-Structured Au/Pd Nanoclusters as Novel Catalysts for Aerobic Glucose Oxidation. *J. Nanosci. Nanotechnol.* **2013**, *13*, 5405−5412.
(21) Jennings, P. C.; Aleksandrov, H. A.; Neyman, K. M.; Johnston, R. L. A DFT Study of Oxygen Dissociation on Platinum Based Nanoparticles. *Nanoscale* **2014**, *6*, 1153−1165.
(22) Jennings, P. C.; Aleksandrov, H. A.; Neyman, K. M.; Johnston, R. L. O2 Dissociation on M@Pt Core-Shell Particles for 3d, 4d, and 5d Transition Metals. *J. Phys. Chem. C* **2015**, *119*, 11031−11041.
(23) He, D. S.; He, D.; Wang, J.; Lin, Y.; Yin, P.; Hong, X.; Wu, Y.; Li, Y. Ultrathin Icosahedral Pt-Enriched Nanocage with Excellent Oxygen Reduction Reaction Activity. *J. Am. Chem. Soc.* **2016**, *138*, 1494−1497.
(24) Wang, X.; Figueroa-Cosme, L.; Yang, X.; Luo, M.; Liu, J.; Xie, Z.; Xia, Y. Pt-Based Icosahedral Nanocages: Using a Combination of {111} Facets, Twin Defects, and Ultrathin Walls to Greatly Enhance Their Activity Toward Oxygen Reduction. *Nano Lett.* **2016**, *16*, 1467−1471.
(25) Wang, X.; Choi, S.-I.; Roling, L. T.; Luo, M.; Ma, C.; Zhang, L.; Chi, M.; Liu, J.; Xie, Z.; Herron, J. A.; Mavrikakis, M.; Xia, Y. Palladium-Platinum Core-Shell Icosahedra with Substantially Enhanced Activity and Durability Towards Oxygen Reduction. *Nat. Commun.* **2015**, *6*, 7594.
(26) Wang, X.; Vara, M.; Luo, M.; Huang, H.; Ruditskiy, A.; Park, J.; Bao, S.; Liu, J.; Howe, J.; Chi, M.; Xie, Z.; Xia, Y. Pd@Pt Core-Shell Concave Decahedra: A Class of Catalysts for the Oxygen Reduction Reaction with Enhanced Activity and Durability. *J. Am. Chem. Soc.* **2015**, *137*, 15036−15042.
(27) Yang, Y.; Zhao, Z.; Cui, R.; Wu, H.; Cheng, D. Structures, Thermal Stability, and Chemical Activity of Crown-Jewel-Structured Pd-Pt Nanoalloys. *J. Phys. Chem. C* **2015**, *119*, 10888−10895.
(28) Vara, M.; Roling, L. T.; Wang, X.; Elnabawy, A. O.; Hood, Z. D.; Chi, M.; Mavrikakis, M.; Xia, Y. Understanding the Thermal Stability of Palladium-Platinum Core-Shell Nanocrystals by In Situ Transmission Electron Microscopy and Density Functional Theory. *ACS Nano* **2017**, *11*, 4571−4581.
(29) Huang, R.; Wen, Y.-H.; Zhu, Z.-Z.; Sun, S.-G. Two-Stage Melting in Core-Shell Nanoparticles: An Atomic-Scale Perspective. *J. Phys. Chem. C* **2012**, *116*, 11837−11841.
(30) Huang, R.; Wen, Y.-H.; Zhu, Z.-Z.; Sun, S.-G. Pt-Pd Bimetallic Catalysts: Structural and Thermal Stabilities of Core-Shell and Alloyed Nanoparticles. *J. Phys. Chem. C* **2012**, *116*, 8664−8671.
(31) Sanchez, S. I.; Small, M. W.; Zuo, J.-m.; Nuzzo, R. G. Structural Characterization of Pt−Pd and Pd−Pt Core−Shell Nanoclusters at Atomic Resolution. *J. Am. Chem. Soc.* **2009**, *131*, 8683−8689.
(32) Anderson, R. M.; Zhang, L.; Loussaert, J. A.; Frenkel, A. I.; Henkelman, G.; Crooks, R. M. An Experimental and Theoretical Investigation of the Inversion of Pd@Pt Core@Shell Dendrimer-Encapsulated Nanoparticles. *ACS Nano* **2013**, *7*, 9345−9353.

DOI: 10.1021/acs.jpcc.8b04177
J. Phys. Chem. C 2018, 122, 18070−18076

(33) An, W.; Liu, P. Size and Shape Effects of Pd@Pt Core-Shell Nanoparticles: Unique Role of Surface Contraction and Local Structural Flexibility. *J. Phys. Chem. C* **2013**, *117*, 16144−16149.
(34) Plimpton, S. Fast Parallel Algorithms for Short-Range Molecular Dynamics. *J. Comp. Physiol.* **1995**, *117*, 1−19.
(35) Chepkasov, I. V.; Gafner, Y. Y.; Gafner, S. L. Synthesis of Cu Nanoparticles by Condensation from the Gas Phase. *Phase Transitions* **2017**, *90*, 590−597.
(36) Chepkasov, I. V.; Gafner, Y. Y.; Gafner, S. L. Changing of the Shape and Structure of Cu Nanoclusters Generated from a Gas Phase: MD Simulations. *J. Aerosol Sci.* **2016**, *91*, 33−42.
(37) Chepkasov, I. V.; Gafner, Y. Y.; Gafner, S. L.; Bardakhanov, S. P. The General Mechanisms of Cu Cluster Formation in the Processes of Condensation from the Gas Phase. *Bull. Mater. Sci.* **2015**, *38*, 701−706.
(38) Berry, R. S.; Smirnov, B. M. Modeling of Configurational Transitions in Atomic Systems. *Phys.-Usp.* **2013**, *56*, 973−998.
(39) Chepkasov, I. V.; Gafner, Y. Y.; Gafner, S. L.; Bardahanov, S. P. Condensation of Cu Nanoparticles from the Gas Phase. *Phys. Met. Metallogr.* **2016**, *117*, 1003−1012.
(40) Polukhin, V. A.; Vatolin, N. A. Stability and Thermal Evolution of Transition Metal and Silicon Clusters. *Russ. Chem. Rev.* **2015**, *84*, 498−539.
(41) Zhou, X. W.; Johnson, R. A.; Wadley, H. N. G. Misfit-Energy-Increasing Dislocations in Vapor-Deposited CoFe/NiFe Multilayers. *Phys. Rev. B: Condens. Matter Mater. Phys.* **2004**, *69*, 144113−144122.
(42) Yun, K.; Cha, P. R.; Lee, J.; Kim, J.; Nam, H. S. Atomistic Simulations of the Structures of Pd-Pt Bimetallic Nanoparticles and Nanowires. 2015, arXiv:1502.07372. arXiv.org e-Print archive. https://arxiv.org/abs/1502.07372 (accessed July 5, 2018).
(43) Michalka, J. R.; Gezelter, J. D. Island Formation on Pt/Pd (557) Surface Alloys in the Presence of Adsorbed CO: A Molecular Dynamics Study. *J. Phys. Chem. C* **2015**, *119*, 14239−14247.
(44) Nosé, S. A molecular dynamics method for simulations in the canonical ensemble. *Mol. Phys.* **1984**, *52*, 255−268.
(45) Nosé, S. A unified formulation of the constant temperature molecular dynamics methods. *J. Phys. Chem.* **1984**, *81*, 511−519.
(46) Hoover, W. G. *Time Reversibility, Computer Simulation, and Chaos*; World Scientific: Singapore, 1999.
(47) Kittel, C.; Kroemer, H.; Scott, H. L. *Thermal Physics*, 2nd ed; W. H. Freeman Company, 1980.
(48) He, Q. F.; Ye, Y. F.; Yang, Y. The configurational entropy of mixing of metastable random solid solution in complex multi-component alloys. *J. Appl. Phys.* **2016**, *120*, 154902.
(49) http://www.openmx-square.org (accessed July 5, 2018).
(50) Morrison, I.; Bylander, D. M.; Kleinman, L. Nonlocal Hermitian Norm-Conserving Vanderbilt Pseudopotential. *Phys. Rev. B: Condens. Matter Mater. Phys.* **1993**, *47*, 6728−6731.
(51) Vanderbilt, D. Soft Self-Consistent Pseudopotentials in a Generalized Eigenvalue Formalism. *Phys. Rev. B: Condens. Matter Mater. Phys.* **1990**, *41*, 7892−7895.
(52) Henkelman, G.; Arnaldsson, A.; Jónsson, H. A fast and Robust Algorithm for Bader Decomposition of Charge Density. *Comput. Mater. Sci.* **2006**, *36*, 254−360.
(53) Stukowski, A. Visualization and analysis of atomistic simulation data with OVITO-the Open Visualization Tool. *Modell. Simul. Mater. Sci. Eng.* **2009**, *18*, 015012.
(54) Momma, K.; Izumi, F. VESTA 3 for three-dimensional visualization of crystal, volumetric and morphology data. *J. Appl. Crystallogr.* **2011**, *44*, 1272−1276.
(55) Polukhin, V. A.; Gafner, Y. Y.; Chepkasov, I. V.; Kurbanova, E. D. Comparative Analysis of the Thermosize Effects of Transition-Metal Clusters that are Free or Deposited onto Graphene. Molecular Dynamics Simulation. *Russ. Metall.* **2014**, *2014*, 112−125.
(56) Paz-Borbón, L. O.; Mortimer-Jones, T. V.; Johnston, R. L.; Posada-Amarillas, A.; Barcaro, G.; Fortunelli, A. Structures and energetics of 98 atom Pd-Pt nanoalloys: potential stability of the Leary tetrahedron for bimetallic nanoparticles. *Phys. Chem. Chem. Phys.* **2007**, *9*, 5202−5208.
(57) Massen, C.; Mortimer-Jones, T. V.; Johnston, R. L. Geometries and segregation properties of platinum-palladium nanoalloy clusters. *J. Chem. Soc.* **2002**, *23*, 4375−4388.
(58) Ishimoto, T.; Koyama, M. Electronic Structure and Phase Stability of PdPt Nanoparticles. *J. Phys. Chem. Lett.* **2016**, *7*, 736−740.
(59) Bernardi, F.; Alves, M. C. M.; Traverse, A.; Silva, D. O.; Scheeren, C. W.; Dupont, J.; Morais, J. Monitoring Atomic Rearrangement in PtxPd1−x (x = 1, 0.7, or 0.5) Nanoparticles Driven by Reduction and Sulfidation Processes. *J. Phys. Chem. C* **2009**, *113*, 3909−3916.
(60) Tyson, W. R.; Miller, W. A. Surface Free Energies of Solid Metals: Estimation From Liquid Surface Tension Measurements. *Surf. Sci.* **1977**, *62*, 267−276.
(61) Paes, V. Z. C.; Castegnaro, M. V.; Baptista, D. L.; Grande, P. L.; Morais, J. Unveiling the Inner Structure of PtPd Nanoparticles. *J. Phys. Chem. C* **2017**, *121*, 19461−19466.
(62) Nguyen, V. L.; Ohtaki, M.; Matsubara, T.; Cao, M. T.; Nogami, M. New Experimental Evidences of Pt-Pd Bimetallic Nanoparticles with Core-Shell Configuration and Highly Fine-Ordered Nanostructures by High-Resolution Electron Transmission Microscopy. *J. Phys. Chem. C* **2012**, *116*, 12265−12274.
(63) Long, N. V.; Ohtaki, M.; Hien, T. D.; Randy, J.; Nogami, M. A comparative study of Pt and Pt-Pd core-shell nanocatalysts. *Electrochim. Acta* **2011**, *56*, 9133−9143.
(64) Chepkasov, I. V.; Gafner, Y. Y.; Vysotin, M. A.; Redel', L. V. A study of melting of various types of Pt-Pd nanoparticles. *Phys. Solid State* **2017**, *59*, 2076−2081.
(65) Patra, A.; Bates, J.; Sun, J.; Perdew, J. P. Properties of Real Metallic Surfaces: Effects of Density Functional Semilocality and Van der Waals Nonlocality. 2017, arXiv:1702.08515. arXiv.org e-Print archive. https://arxiv.org/abs/1702.08515 (accessed July 5, 2018).
(66) Wang, J.; Liu, D.; Li, L.; Qi, X.; Xiong, K.; Ding, W.; Chen, S.; Wei, Z. Origin of the Enhanced Catalytic Activity of PtM/Pd (111) with Doped Atoms Changing from Chemically Inert Au to Active Os. *J. Phys. Chem. C* **2017**, *121*, 8781−8786.
(67) Wang, J. X.; Inada, H.; Wu, L.; Zhu, Y.; Choi, Y. M.; Liu, P.; Zhou, W.-P.; Adzic, R. R. Oxygen Reduction on Well-Defined Core−Shell Nanocatalysts: Particle Size, Facet, and Pt Shell Thickness Effects. *J. Am. Chem. Soc.* **2009**, *131*, 17298−17302.

DOI: 10.1021/acs.jpcc.8b04177
J. Phys. Chem. C 2018, 122, 18070−18076